Nanoscale

Accepted Manuscript

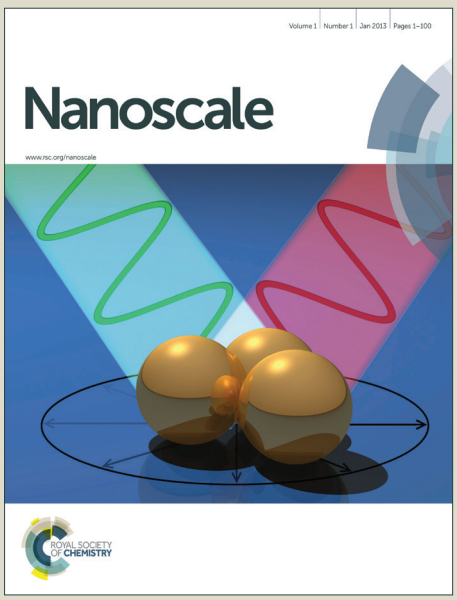

ROYAL SOCIETY OF CHEMISTRY

www.rsc.org/nanoscale

Nanoscale

RSCPublishing

ARTICLE

Vertical junction photodetectors based on reduced graphene oxide/silicon Schottky diodes

Cite this: DOI: 10.1039/x0xx00000x

Miao Zhu,[a,b] Xinming Li,[c] Yibo Guo,[d] Xiao Li,[a,b] Pengzhan Sun,[a] Xiaobei Zang,[a] Kunlin Wang,[a] Minlin Zhong,[a] Dehai Wu,[d] Hongwei Zhu*[a,b]

Received 00th January 2014,
Accepted 00th January 2014

DOI: 10.1039/x0xx00000x

www.rsc.org/

Reduced graphene oxide (RGO) has been employed as the electrode for a series of vertically structured photodetectors. Comparing with the mechanically exfoliated or chemical vapor deposited graphene, RGO possesses more oxygen containing groups and defects, which are proved to be favorable to enhance the performance of photodetectors. As a matter of fact, RGO with different reduction levels can be readily obtained by varying the annealing process. The synthetic procedures for RGO material are suitable for large scale production, and its performance can be effectively improved by functionalization or element doping. For RGO-based devices, the Schottky junction properties and photoelectric conversion have been investigated, primarily by analyzing their current-voltage characteristics. Subsequently, the ON/OFF ratio, responsivity and detectivity of the photodetectors were closely examined, proving that RGO material could be effectively utilized as the electrode material; plus, their relationship with the RGO reduction levels has also been explored. By analyzing the response/recovery speed of the RGO-based photodetectors, we have studied the effects of oxygen-containing functional groups and crystalline defects on the photoelectric conversion.

Introduction

Graphene, a two dimensional carbon material with high transmittance and carrier transportation rate,[1,2] has been successfully employed in solar cells, presumably by forming a Schottky junction with n-Si.[3-6] In such photovoltaic models, graphene not only works as the transparent conductive layer but also contributes to the carrier separation.[3] Recently, An et al.[7], Zhang et al.[8] and Lv et al.[9] have extended this model to the development of photodetectors, and they have found that these devices exhibited excellent performance, indicating this should be a promising field for graphene application. On the other hand, recent reports have demonstrated that n-Si could be substituted with other types of material, for instance, both traditional semiconductor like germanium and CdSe,[10,11] and the new two dimensional transition-metal dichalcogenide material possessing semiconducting properties like MoS_2, have been used for this purpose.[12-15] However, a vast majority of the electrode material used is either mechanically exfoliated (ME) or chemical vapor deposited (CVD) graphene, which is often prepared via complicated processes with low productivity. It has been proved that element doping[16-19] and functionalization[20-23] are important approaches to effectively modify or improve graphene properties. But for graphene prepared by ME/CVD processes, only a few elements can be doped, and the resulting content is generally fairly low. Most of the functionalized graphene has been synthesized via approaches involving graphene oxide (GO). Consequently, using the reduced GO (RGO) as electrode material for Schottky diode photodetectors would be of great importance. The most critical difference between RGO material and ME/CVD graphene is that the former contains a large amount of oxygen-containing functional groups (OFGs) and defects, which naturally would impose additional influences on the performance of photodetectors.

In this work, a series of RGO/n-Si Schottky diode photodetectors have been constructed, and their photo-detecting performance was closely examined. Particularly, the relationship between the junction properties and the reduction levels of graphene oxide was also explored, and it appears that the reduction levels could substantially affect the performance of photodetectors. Upon optimizatoin, the overall performance can be adjusted to be much better than CVD graphene based devices.

Experimental

Fabrication of the devices

Water-dispersed GO (0.25mg/mL, purchased from Nanjing XFNANO Materials Tech Co. Ltd.) was firstly dropped onto n-Si substrate with SiO_2 layer deposited along the border of the surface. After dried in air for several minutes, the substrate with GO was placed into a quartz tube and annealed at different temperatures with the protection of Ar and H_2 (20:1 in flow rate) for 30 min to reduce GO to different levels. After annealing, the SiO_2 side of the substrate was treated by HF (40 wt.%) evaporation for 2~3 min to remove the SiO_2 layer which was formed during the annealing process. Then a mixture of indium and germanium was coated on the other side of the substrate to serve as the back electrode. Finally the substrate was stuck to a Cu tape to form a photodetector device.

Characterizations

The power density of the laser was measured by Sanwa LP1. Raman spectra were collected by Reinshaw 2000 with a 514 nm laser source. The transmittances of RGO films were measured by Agilent Cary 5000. The *I-V* characteristics were tested by Keithley 2601.

Results and discussion

The construction process and the detailed structure of photodetectors have been shown in Figure 1. At first, an aqueous GO dispersion was dropped on the surface of an n-Si wafer with SiO_2 coatings, forming a continuous film; subsequently, the film was reduced by annealing process in a quartz tube. Notably, the level of reduction can be tuned by controlling the annealing temperature. After that, the resulting wafer was treated with HF (40 wt.%), and followed by evaporation to remove the SiO_2 layers presiding on the n-Si material, largely formed during the annealing process. Finally, the In/Ga back electrode was attached to the back side of the wafer, and then a copper tape was attached to the In/Ga electrode, eventually furnishing a complete photodetector.

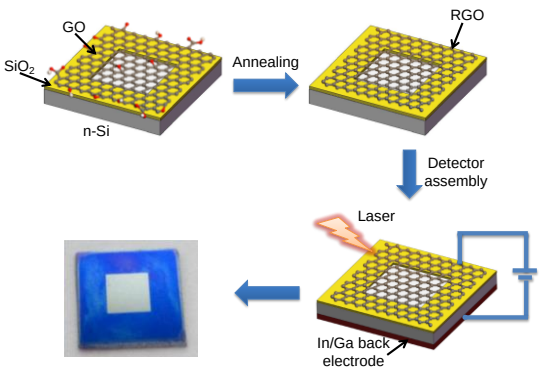

Figure 1. Structure and fabrication process of RGO/n-Si photodetector.

During the course of reduction, certain OFGs can be dissociated from the GO basal plane, thus the morphology and properties of GO could be significantly altered. Indeed, as demonstrated in Figure 2a, the sheet resistance of RGO films has been dramatically decreased with the increase of reduction temperature, presumably because the number of delocalized π bonds for sp^2 carbons was increased by the reduction.[24] Theoretically, lower sheet resistance for electrodes should be beneficial to the separation and transportation of photo-carriers. On the other hand, the reduction of GO can only slightly affect the transmittance of the RGO films, thus its influences on the generation of photo-carriers in n-Si material should be trivial, as shown in Figure 2b. However, higher reduction level is not always beneficial for the photoelectric conversion. When RGO was reduced at high annealing temperature, the corresponding Raman spectra have been collected, as shown in Figure 2c. It appears that the ratio of I_D/I_G rose systematically when the temperature was increased from 200 ℃ to 500 ℃.

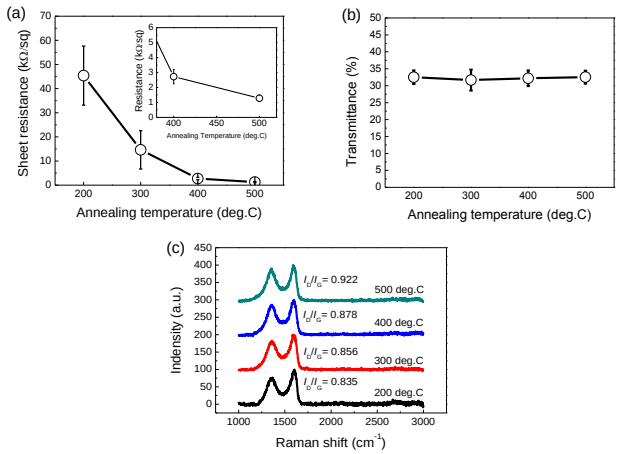

Figure 2. Influence of reduction on RGO films. (a) Sheet resistance: declines significantly, the inset shows the enlarged view of 400~500°C range, (b) Transmittance: slightly fluctuates around 32% and (c) Raman spectrum: I_D/I_G arises with further reduction, indicating the increase of crystalline defects in RGO.

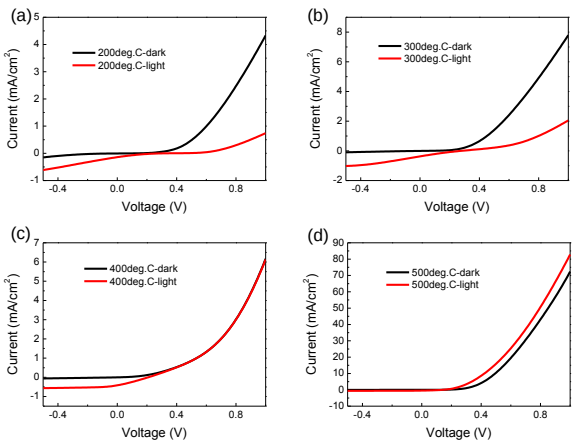

Figure 3. (a-d) Dark and light characteristics of the photodetectors annealing at 200, 300, 400 and 500°C, respectively. All devices have displayed excellent rectification effects with low leakage current and obvious reflection on illumination.

These results indicate that the reduction process has led to the degradation of the graphitic carbon, which is considered as one of the structural defects in RGO material.[24,25] To obtain accurate reduction levels, X-ray photoelectron spectroscopy (XPS) analysis has been performed to determine the oxygen content in RGO films, as illustrated in Figure S1. Specifically, it was found that the oxygen content has been reduced from 19.2% to 11.1%, proving that thermal treatment is effective for reducing GO.

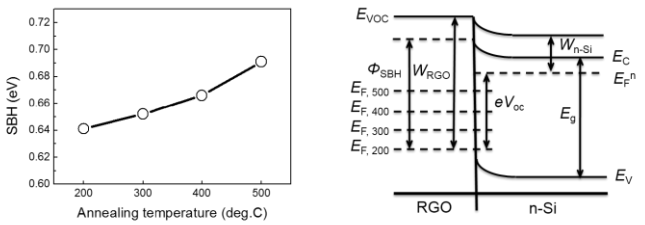

Figure 4. (a) Relationship between SBH and the reduction level of RGO. (b) Band diagram of the RGO/n-Si interface.

With these results in hand, we next investigated the photovoltaic properties of the RGO/n-Si Schottky junctions. Particularly, a series of RGO-based photodetectors with different reduction levels were illuminated by a 445 nm laser beam, at a 7.45 mW/cm^{2}power density. Particularly, both dark and illuminated current-voltage characteristics have been studied, and the results were summarized in Figure 3. Notably, in the dark current curves obtained, decent rectification effects with low leakage current were evident; upon laser illuminating, however, all devices showed remarkable reactions, as demonstrated by the light current-voltage (*I-V*) curves. To further understand the intrinsic properties of diodes, the Schottky barrier height (SBH) has been determined, using the following thermionic-emission based diode equation:[10]

$$J(T,V) = J_s(T)(e^{\frac{qV}{\eta\kappa_B T}} - 1) = A^* T^2 e^{-\frac{q\phi_{SBH}}{\kappa_B T}} (e^{\frac{qV}{\eta\kappa_B T}} - 1)$$

where J, J_s, η, κ_B, T, V and $A^*$are current density across the RGO/n-Si interface, saturation current density, ideality factor, Boltzmann's constant, absolute temperature, applied bias voltage and Richardson constant, respectively. For n-Si material, A^* is 112 A cm^{-2} K^{-2}, thus the corresponding Schottky barrier height ϕ_{SBH} has been determined, as illustrated in Figure 4a. According to the classical theory of Schottky contact, if no other factors were taken into account, SBH should be only dependent on the work function of RGO (W_{RGO}), as expressed by the following equation,

$$\phi_{SBH} = W_{RGO} - \chi$$

where χ is the electronic affinity of n-Si. However, for RGO material, it has been reported that its work function increases with the rise of oxygen content,[26] contradictory to the evolution trend illustrated in Figure 4b. Possibly, the surface state of n-Si could be strongly influenced by the presence of enormous amounts of OFGs and dangling bonds on the RGO surface, because they can shield the effects of the work function of RGO, markedly. Furthermore, as SBH of RGO/n-Si junction increases with the RGO reduction level, its potential could also lead to the surface state change of n-Si, which should favor the SBH reduction. Consequently, a higher SBH generally implies that the built-in electric field in the junction is adequately strong, which would be beneficial to the separation of photo-carriers.[27,28]

To investigate the carrier transport processes near the RGO/n-Si interface, ideality factors of the junctions were calculated by the following equation, [10,30]

$$\eta = \left(\frac{q}{kT}\right)\left(\frac{dV}{d\ln I_d}\right)$$

where η, q, k, T, V and I_d are ideality factor, electron charge, Boltzmann constant, absolute temperature, bias voltage and dark current, respectively. As shown in Figure 5, the ideality factors decreased from 3.98 to 2.03, gradually approaching to its normal range ($1<n<2$),[29] which indicates an increasing conformity to an ideal thermionic emission diodes.

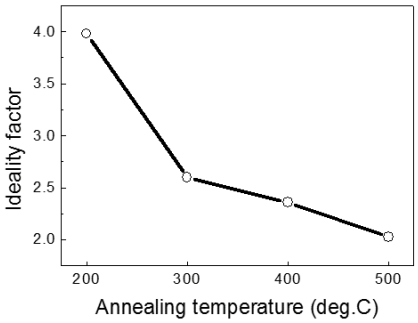

Figure 5. Ideality factor vs. annealing temperature.

In addition, the property of photoelectric conversion has also be evaluated using the *I-V* characteristics such as the open circuit voltage (V_{oc}), short circuit current (I_{sc}), fill factor (FF), and power conversion efficiency (PCE), and the results were shown in Figure 6. Particularly, V_{oc} is the direct monitor for photovoltage, which is generated by the separated electron-hole pairs excited by incident light. Because the transmittance variations due to RGO reduction are negligible, the most critical factor affecting V_{oc} is deemed to be the separation process of photo-carriers. If accumulated enough, crystal defects in RGO such as dislocations, vacancies and impurities are known to significantly promote the recombination of electrons and holes, therefore, V_{oc} should decline with the increase of reduction levels, as shown in Figure 6a. Theoretically, I_{sc} is related to both the generation and transportation of photo-carriers. Even though the recombination of electrons and holes can be dramatically enhanced by extensive reduction, the scattering effects to photo-carriers due to OFGs[31] would be weakened. Consequently, the transportation resistance should be decreased, resulting in an increase of I_{sc}, as demonstrated in Figure 6b. Fill factor (FF) is the crucial parameter to measure the "squareness" of *I-V* characteristics, and it is often in conjunction with V_{oc} and I_{sc}; typically, FF can be affected by both series resistance and shunt resistance of devices. As shown in Figure 6c, GO reduction has substantially improved the FF of devices, which ultimately should enhance their efficiency of energy utilization. PCE, another important factor representing the performance of photoelectric devices, is a combinational effect of V_{oc}, I_{sc} and FF. As shown in Figure 6d,when the annealing temperature was increased from 200 to 300°C, substantial enhancement was evident in the PCE obtained. However, when the annealing temperature was allowed to rise continuously, the PCE obtained did not increase along, instead, it stabilized at ca. 0.31%; possibly, this unusual tendency is due to the mixed effect from the decreasing V_{oc} and increasing I_{sc}, eventually reaching an equilibrium. At this stage, it appears that the photoelectric conversion efficiency of these devices is relatively low, possibly unsuitable for solar cells; however, further study showed that they are ideal for photodetectors.

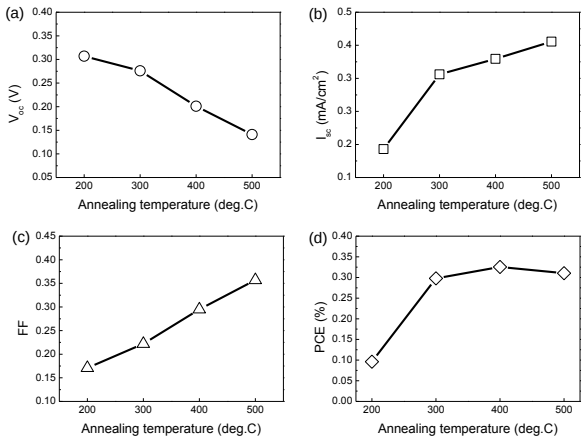

Figure 6. Typical photoelectric conversion properties of the device. (a) V_{oc}: decreases as reduction progressing, (b) I_{sc} and (c) FF: arise as reduction progressing, (d) Power conversion efficiency: arises at the beginning, and then stabilizes at ca. 0.31%.

The photoresponse of devices has been closely examined by exposing to a 445 nm laser beam, the same equipment used in the previous studies, except a different bias voltage (0 and -0.5 V) was applied. The results obtained were summarized in Figure 7. Notably, all devices have exhibited high ON/OFF ratios (above 10^4) at the zero bias voltage; when a -0.5 V bias voltage was applied, the ON/OFF ratios declined severely, possibly due to the increase of dark current, even though the photocurrent has been enhanced to certain extent. On the other hand, for the device using RGO material reduced at 200°C, its dark current possessed obvious noises, and the device also exhibited poor stability, as shown in Figure 7a.

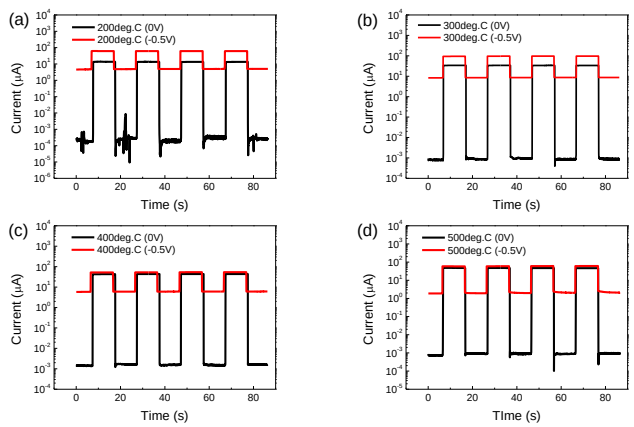

Figure 7. Comparison of the photoresponse while annealing at (a) 200 °C, (b) 300 °C, (c) 400 °C and (d) 500 °C. All devices have displayed excellent ON/OFF ratios (>10^4) at a zero bias voltage, but significantly declined when a -0.5 V bias voltage was applied.

Possibly, this is caused by the strong scattering effect to the carriers from OFGs, and it can be mitigated effectively by further reduction (Figures 7b-d). To evaluate the detection performance of the devices constructed, the corresponding ON/OFF ratio, responsivity and detectivity have been determined, and the results were summarized in Table 1. Specifically, R_A and D^*can be calculated using the following equations,[10,32]

$$R_A = I_P / P \quad , \qquad D^* = R_A A^{1/2} (2qI_d)^{-1/2}$$

where I_P, P, q, A and I_d are photocurrent, laser power, electron charge, active area and dark current, respectively.

Table 1. Typical photoelectric properties of the RGO/n-Si photodetectors.

T (°C)	I_{light}/I_{dark} (ON/OFF Ratio)		R_A (mA/W)		D^*(cm Hz$^{1/2}$ W^{-1})	
	0V	-0.5V	0V	-0.5V	0V	-0.5V
200	6.25×10^4	12.61	18.12	82.42	6.89×10^{11}	2.09×10^{10}
300	3.74×10^4	11.23	45.23	128.72	8.42×10^{11}	2.46×10^{10}
400	2.76×10^4	8.89	58.12	71.28	8.20×10^{11}	1.63×10^{10}
500	5.23×10^4	29.31	62.95	80.27	11.76×10^{11}	3.14×10^{10}

Notably, the ON/OFF ratios and detectivity are fluctuating around $(2.76\sim6.25)\times10^4$ and $(6.89\sim11.76)\times10^{11}$ cm Hz$^{1/2}$ W^{-1} at zero bias, respectively, apparently not relating to the reduction levels. Photocurrent can be improved by adjusting reduction levels to a limited extent; however, it could also be dramatically affected by dark current, which is sensitive to various complications such as SBH, sheet resistance and the interface of RGO/n-Si. Different from the ON/OFF ratio and detectivity, the device responsivity has exhibited a progressive increase along with the reduction level, which should be a reasonable outcome of the increasing I_{sc}. For most of the photodetector devices, applying a bias voltage is an effective way to enhance the responsivity, because the transportation of photo-carriers can be promoted by external electric potential field. Therefore, we have applied a -0.5V bias voltage on the devices prepared in our laboratory, in the hope of getting better performance. Surprisingly, even though slight improvement was evident in the device responsivity, the ON/OFF ratio and detectivity have been severely reduced, appropriately two orders of magnitude less than the original (Table 1). Therefore, we conclude that an extra bias voltage could not be employed to improve the performances of RGO/n-Si photodetectors.

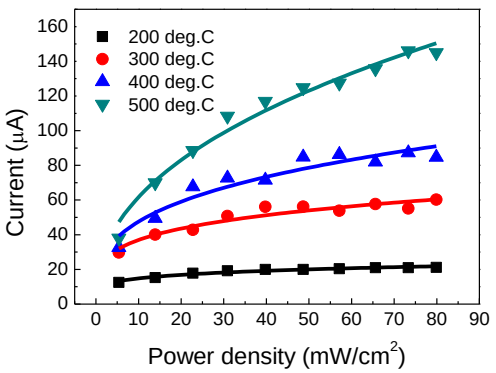

Figure 8. Photocurrent dependence on the intensity of incident light. The curves have been fitted by equation: $I = AP^{\vartheta}$. The exponent ϑ is 0.187, 0.236, 0.313 and 0.429, respectively, indicating that the trapping effects on the photo-carriers are originated from the OFGs.

Under different incident light power densities, the device photocurrents have been measured, as shown in Figure 8. Notably, an increasing tendency was evident in the photocurrents

of all devices, which essentially can be described by the following equation,[10,33,34]

$$I = AP^{\theta}$$

where I is the photocurrent, A is a constant under certain wavelength, P is the power density of the incident light and θ is the parameter relating to the trapping and recombination process of the photo-carriers in photodetectors,[34,35] which can be obtained by fitting the *I-P* curves, as summarized in Table 2.

Table 2. Fitting results of the exponent θ for the curves shown in Figure 7.

T (°C)	200	300	400	500
θ	0.187	0.236	0.313	0.429

Particularly, when the reduction level of RGO was increased, the amount of OFGs naturally would decrease, and θ seemed to further approach an integer, indicating that the trapping and recombination during the transportation of photo-carriers have been weakened.[10] Therefore, we conclude that GO reduction should be a viable approach to improve the linearity of the photocurrent response towards the incident light intensity.

We next examined the response and recovery speed of the RGO photodetectors, in an effort to further understand the effect of OFGs and crystal defects. Notably, it was found that a proper time of reduction can effectively shorten the response time of a RGO device; however, it appeared that excessive reduction would prolong it, conversely (Figure 9a). Possibly, this is because OFGs and crystal defects play different roles in the photoelectric conversion process. As demonstrated in Figure S2, for RGO with low reduction level (200°C), the rising edge is consisted of a sharp rising front and a mild growth tail, which indicates that the generation and separation process of photo-carriers are rapidly proceeding, but the transportation process is not stable yet.

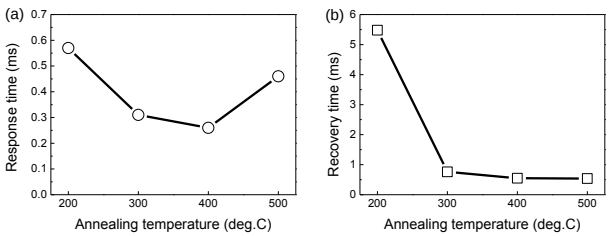

Figure 9. Response/recovery time dependence on the reduction level. (a) Excessive reduction did not shorten the response time, (b) but further reduction can improve the recovery speed.

However, for RGO with a high reduction level (500°C), the result is opposite. Possibly, OFGs mainly contribute to the scattering of photo-carriers, which consequently would impede the establishment of a stable voltage; crystal defects, on the other hand, tend to enhance the recombination process during the generation and separation of photo-carriers. Naturally, for RGO with an appropriate reduction level, for instance, annealed at 300 and 400°C, the device response speed can be relatively improved. Different from the response to illumination, the recovery process is a complete recombination process of photo-carriers. As shown in Figure S3, the V_{oc} of the devices are decayed in exponential, which are in consistent with the low injection conditions,[36] indicating the photocurrent in our devices are mainly contributed by the holes excited from the illumination. Concerned with the carriers lifetime, the recovery speed can be improved by reduction to some extent (Figure 9b), but cannot be ameliorated any more just by further reduction when a limit is reached.

Our results show that the overall performance of the RGO/Si devices can be improved by appropriate GO reduction. Table 3 compares the typical photodetecting performance between CVD graphene/Si and RGO/Si photodetectors.

Table 3. Comparison of typical photodetecting performance between CVD graphene and RGO based photodetectors

Electrode	ON/OFF Ratio	R_A (mA/W)	D^* (cm $Hz^{1/2}$ W^{-1})	Response Time (ms)	Recovery Time (ms)
CVD Graphene[6]	~ 1×10^4	200	7.69×10^9	1.2	3
RGO	2.76~6.25 $\times10^4$	18.12~128.72	6.89~11.76 $\times10^{11}$	0.26	0.54

Conclusions

In conclusion, we have proved that RGO material can effectively substitute ME/CVD graphene in the construction of n-Si Schottky heterojunction photodetectors, and the resulting devices have exhibited excellent photo-detecting properties such as ON/OFF ratio, responsivity and detectivity. Particularly, OFGs and crystal defects in RGO material can influence various device properties, presumably by scattering, trapping or enhancing the recombination of the excited electron-hole pairs. It was found that altering the reduction levels of RGO can modulate vectors such as SBH, I_{sc}, FF, PCE, V_{oc} and the responsivity at zero bias; however, it can barely affect the ON/OFF ratios or detectivity. Moreover, even though applying a bias voltage can enhance the device responsivity to certain extent, it also results in sharp decrease of ON/OFF ratios and detectivity, proving that a bias voltage would not be able to improve device performance. Finally, we have found that during the photoelectric conversion process, OFGs and crystalline defects mainly influence the transportation of photo-carriers, possibly by scattering, separation, or enhanced recombination.

Acknowledgements

This work is supported by National Science Foundation of China (51372133), Tsinghua National Laboratory for Information Science and Technology (TNList) Cross-discipline Foundation, National Program on Key Basic Research Project (2011CB013000, 2013CB934201), Tsinghua University Initiative Scientific Research Program (2012Z02102).

Notes and references

[a] School of Materials Science and Engineering, State Key Laboratory of New Ceramics and Fine Processing, Key Laboratory of Materials Processing Technology of MOE, Tsinghua University, Beijing 100084, China.

[b] Center for Nano and Micro Mechanics, Tsinghua University, Beijing 100084, China.

[c] National Center for Nanoscience and Technology, Zhongguancun, Beijing100190, China.

[d] Department of Mechanical Engineering, Tsinghua University, Beijing 100084, China.

Electronic Supplementary Information (ESI) available: XPS spectra of RGO films, response and recovery processes of RGO/Si devices. See DOI: 10.1039/b000000x/

1 K. S. Novoselov, A. K. Geim, S. V. Morozov, D. Jiang, Y. Zhang, S. V. Dubonos, I. V. Grigorieva and A. A. Firsov, *Science*, 2004, **306**, 666.
2. A. K. Geim and K. S. Novoselov, *Nat. Mater.*, 2007, **6**, 183.
3. X. Li, H. Zhu, K. Wang, A. Cao, J. Wei, C. Li, Y. Jia, Z. Li, X. Li and D. Wu, *Adv. Mater.*, 2010, **22**, 2743.
4. X. Miao, S. Tongay, M. K. Petterson, K. Berke, A. G. Rinzler, B. R. Appleton and A. F. Hebard, *Nano Lett.*, 2012, **12**, 2745.
5. E. Shi, H. Li, L. Yang, L. Zhang, Z. Li, P. Li, Y. Shang, S. Wu, X. Li, J. Wei, K. Wang, H. Zhu, D. Wu, Y. Fang and A. Cao, *Nano Lett*., 2013, **13**, 1776.
6. C. Xie, X. Zhang, Y. Wu, X. Zhang, X. Zhang, Y. Wang, W. Zhang, P. Gao, Y. Hana and J. Jie, *J. Mater. Chem. A*, 2013, **1**, 8567.
7. X. An, F. Liu, Y. J. Jung and S. Kar, *Nano Lett.*, 2013, **13**, 909.
8. Z. Zhang, Y. Guo, X. Wang, D. Li, F. Wang and S. Xie, *Adv. Funct. Mater*. 2014, **24**, 835.
9. P. Lv, X. Zhang, X. Zhang, W. Deng and J. Jie, *IEEE Elect. Dev. Lett.*, 2013, **34**, 1337.
10. L. Zeng, M. Wang, H. Hu, B. Nie, Y. Yu, C. Wu, L. Wang, J. Hu, C. Xie, F. Liang and L. Luo, *ACS Appl. Mater. Interfaces*, 2013, **5**, 9362.
11. Z. Gao, W. Jin, Y. Zhou, Y. Dai, B. Yu, C. Liu, W. Xu, Y. Li, H. Peng, Z. Liu and L. Dai, Nanoscale, 2013, **5**, 5576.
12. D. Jariwalaa, V. K. Sangwana, C. Wua, P. L. Prabhumirashia, M. L. Geiera, T. J. Marksa, L. J. Lauhona and M. C. Hersama, *PNAS*, 2013, **110**, 18076.
13. K. Roy, M. Padmanabhan, S. Goswami, T. P. Sai, G. Ramalingam, S. Raghavan and A. Ghosh, *Nat. Nano*., 2013, **8**, 826.
14. W. J. Yu, Y. Liu, H. Zhou, A. Yin, Z. Li, Y. Huang and X. Duan, *Nat. Nano*., 2013, **8**, 952.
15. O. Lopez-Sanchez, D. Lembke, M. Kayci, A. Radenovic and A. Kis, *Nat. Nano.*, 2013, **8**, 497.
16. D. Wei, Y. Liu, Y. Wang, H. Zhang, L. Huang and G. Yu, *Nano Lett.*, 2009, **9**, 1752.
17. H. Wang, T. Maiyalagan and X. Wang, *ACS Catal.*, 2012, **2**, 781.
18. J. Gebhardt, R. J. Koch, W. Zhao, O. Höfert, K. Gotterbarm, S. Mammadov, C. Papp, A. Görling, H.-P. Steinrück and Th. Seyller, *Phys. Rev. B*, 2013, **87**, 155437.
19. Z. M. Ao, Q. Jiang, R. Q. Zhang, T. T. Tan and S. Li, *J. Appl. Phys.*, 2009, **105**, 074307.
20. A. K. Geim, *Science*, 2009, **324**, 1530-1534.
21. R. K. Layek and A. K. Nandi, *Polymer*, 2013, **54**, 5087-5103.
22. V. Georgakilas, M. Otyepka, A. B. Bourlinos, V. Chandra, N. Kim, K. C. Kemp, P. Hobza, R. Zboril and K. S. Kim, *Chem. Rev*., 2012, **112**, 6156.
23. X. Li, D. Xie, H. Park, M. Zhu, T. H. Zeng, K. Wang, J. Wei, D. Wu, J. Kong and H. Zhu. *Nanoscale*, 2013, **5**, 1945.
24. C. Mattevi, G. Eda, S. Agnoli, S. Miller, K. A. Mkhoyan, O. Celik, D. Mastrogiovanni, G. Granozzi, E. Garfunkel and M. Chhowalla, *Adv. Funct. Mater.*, 2009, **19**, 2577.
25. S. Pei and H. Cheng, *Carbon*, 2012, **50**, 3210.
26. P. V. Kumar, M. Bernardi and J. C. Grossman, *ACS Nano*, 2013, **7**, 1638.
27. Y. Lin, X. Li, D. Xie, T. Feng, Y. Chen, R. Song, H. Tian, T. Ren, M. Zhong, K. Wang and H. Zhu, *Energy Environ. Sci.*, 2013, **6**, 108.
28. X. Li, D. Xie, H. Park, T. H. Zeng, K. Wang, J. Wei, M. Zhong, D. Wu, J. Kong and H. Zhu, Adv. Energy Mater., 2013, **3**, 1029.
29. M. Patel, I. Mukhopadhyay and A. Ray, *Semicond. Sci. Technol*., 2013, **28**, 055001.
30. M. Biber, Ö. Güllü, S. Forment, R. L. Van Meirhaeghe and A. Türüt, *Semicond. Sci. Technol.*, 2006, **21**, 1.
31. S. Pei and H. Cheng, *Carbon*, 2012, **50**, 3210.
32. E. A. Anagnostakis, *Phys. Stat. Sol.(a)*, 1991, **127**, 153.
33. Y. L. Cao, Z. T. Liu, L. M. Chen, Y. B. Tang, L. B. Luo, J. S. Jie, W. J. Zhang, S. T. Lee and C. S. Lee, *Opt. Express*, 2011, **19**, 6100.
34. H. Kind, H. Yan, B. Messer, M. Law and P. Yang, *Adv. Mater*., 2002, **14**, 158.
35. D. Wu, Y. Jiang, Y. Zhang, J. Li, Y. Yu, Y. Zhang, Z. Zhu, L. Wang, C. Wu, L. Luo and J. Jie, *J. Mater. Chem.*, 2012, **22**, 6206.
36. J. E. Mahan, T. W. Ekstedt, R. I. Frank and R. Kaplow, *IEEE Trans. Electr. Dev.*, 1979, **ED-26**, 733.

